Astronomy & Astrophysics manuscript no. 04579
December 10, 2018

Outflow and accretion detections in the young stellar object IRAS 04579+4703

Jin-Long Xu,[1,2] Jun-Jie Wang[1] and Sheng-Li Qin[3]

[1] National Astronomical Observatories, Chinese Academy of Sciences, Beijing 100012, China
e-mail: xujl@bao.ac.cn
[2] Graduate University of the Chinese Academy of Sciences, Beijing, 100080, China

[3] I. Physikalisches Institut, Universität zu Köln, Zülpicher Str. 77, 50937 Köln, Germany

Preprint online version: December 10, 2018

ABSTRACT

We present Submillimeter Array observations of the young stellar object IRAS 04579+4703 in the 1.3 mm continuum and in the ^{12}CO(2 – 1), ^{13}CO(2 – 1) and C^{18}O(2 – 1) lines. The 1.3 mm continuum image reveals a flattened structure with a mass of 13 $M_{\odot}$. The ^{12}CO(2 – 1) line map and position-velocity (PV) diagram, together with the broad wing (full width = 30 km s^{-1}) of ^{12}CO(2 – 1) line, clearly show that there is an outflow motion, which originates from an embedded massive YSO in this region. The lengths of the blue-shifted and red-shifted lobes are 0.14 pc and 0.13 pc respectively. The total gas mass, average dynamical timescale and mass entrainment rate of the outflow are 1.8 $M_{\odot}$, 1.7 × 10^4 yr and 1.1 × 10^{-4} $M_{\odot}$ yr^{-1}, respectively. The flattened morphology of the continuum source perpendicular to the outflow direction, and the velocity gradient seen in the spectra of C^{18}O(2 – 1) taken from different locations along the major axis of the continuum source, suggest the presence of an accretion disk in this region.

Key words. ISM: individual (IRAS 04579+4703) — ISM: kinematics and dynamics — ISM: molecules — stars: formation

1. Introduction

Observational evidences suggest that massive stars may be formed through the accretion-disk-outflow processes similar to low-mass stars (e.g, Shu et al. 1987; Cesaroni et al. 1999; Shepherd et al. 2001;Patel et al. 2005; Jiang et al. 2005; Zinnecker & Yorke 2007). Searching for collapse, accretion and outflow with interferometers in massive star formation regions has boomed (e.g, Beuther e al. 2004; Qin et al. 2008; Furuya et al. 2011), but the limited observations cannot provide detailed information for our understanding of massive star formation. The major difficulty is due to the large distances (≥ 1 kpc), clustered formation environments and shorter evolutionary timescale of massive stars.

IRAS 04579+4703 is a young high mass stellar object (YSO). Molinari et al. (1996) carried out the NH_3 observation toward IRAS 04579+4703, and obtained a distance of 2.47 kpc from the sun and a bolometric luminosity of $3.91\times10^3 L_{\odot}$. However, Molinari et al. (1998a) failed to observe any 6 cm emission from IRAS 04579+4703. Sánchez-Monge et al. (2008) performed higher spatial resolution continuum observations at 1.2 mm, 7 mm, 1.3 cm and 3.6 cm toward IRAS 04579+4703. Their observations showed that the 7 mm emission, similar to the 1.3 cm and 3.6 cm emission in morphology, is elongated in the southwest-northeast direction. The location of their 1.2 mm continuum peak agrees well with that of the source detected at cm wavelengths as well as an H_2O maser (Palla et al. 1991 & Migenes et al. 1999), indicating that the emissions only concentrate on a small and compact region and the IRAS 04579+4703 is at an early evolutionary stage. Using the SED fit, Sánchez-Monge et al. (2008) derived **a** dust temperature of about 30 K and obtained a gas mass of 23 $M_{\odot}$. The line ^{12}CO(2 – 1) observations of Zhang et al. (2005) did not reveal molecular outflow from IRAS 04579+4703, while Wouterloot & Brand (1989) observed the ^{12}CO(1 – 0) emission with a linewidth of 6.1 km s^{-1}. Additionally, Varricatt et al. (2010) detected jet-like H_2 knots in the northwest-southeast direction. However, these observations can not provide sufficient evidences for the outflow. Higher spatial resolution observations of the molecular lines and continuum in submillimeter/millimeter waveband are needed to reveal the detailed source structure and kinematics in this region.

In this paper we present Submillmeter Array (SMA) observations of the young stellar object IRAS 04579+4703 obtained in the 1.3 mm continuum and in the ^{12}CO(2–1), ^{13}CO(2–1), and C^{18}O(2 – 1). Our observations at high angular resolution reveal bipolar outflow motion and gas accretion for IRAS 04579+4703.

2. OBSERVATIONS AND DATA REDUCTION

The observations toward IRAS 04579+4703 were performed with the SMA on 2008 March 21, at 220 (lower sideband) and 230 GHz (upper sideband)[1]. The two sidebands of the SMA covered frequency ranges of 219.4–221.4 GHz and 229.4–231.4 GHz, respectively. The projected baselines ranged from 7 kλ to 100 kλ. The phase track center was R.A.(J2000.0)= $05^h01^m39^s.92$ and Dec.(J2000.0) = 47°07′21″.10. The typical system temperature was 186 K. The spectral resolution is 0.406 MHz, corresponding to a velocity resolution of 0.5 km s^{-1}. The bright quasar 3C279 was used for bandpass calibration, while absolute flux density scales were determined from observations of Titan. QSO 0533+483 and QSO 0359+509 were observed

[1] The data are publicly available on the website http://www.cfa.harvard.edu/rtdc/data/search.html

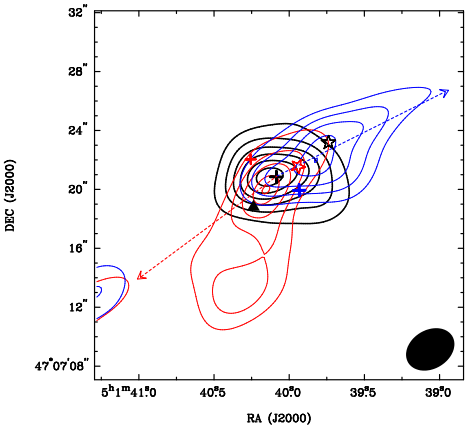

Fig. 1. 1.3 mm continuum emission (black thicker contours) overlaid with the velocity integrated intensity map of ^{12}CO(2−1) outflow (red and blue contours). The black contour levels are at 3, 6, 9, 12, 15, 18 and 21 σ (1 σ is 0.002 Jy beam^{-1}). The red and blue contour levels are 35, 50,..., 95 % of the peak value. The synthesized beam is 3″.49 × 2″.63, P.A.= -58.9° (shown in the lower right corner). The black plus symbol marks the peak position of the continuum source. The blue and red plus symbols represent the positions of the extracted spectra in Fig.4, respectively. H_2O maser is shown with the filled triangle. The black and red open star symbols indicate the location of the infrared source IRAS 04579+4703 and a near-IR source detected by Varricatt et al. (2010), respectively. The blue and red dashed lines mark the direction of the NW and SE lobes of the H_2 knots (Varricatt et al. 2010), respectively.

for antenna gain corrections. The calibration and imaging were performed in Miriad. A continuum image was constructed from the line-free channels. The spectral cubes were constructed using the continuum-subtracted spectral channels. Self-calibration was performed to the continuum data. The gain solutions from the continuum were applied to the line data. The synthesized beam size of the continuum was approximately 3″.49 × 2″.63 with a P.A. =-58°.9. Based on the phase monitoring of QSO 0533+483, the absolution position accuracy (pointing error) is estimated to be ∼0.1″ during the observations.

3. RESULTS

3.1. Continuum Emission at 1.3 mm

In Figure 1, the 1.3 mm continuum image observed with the SMA shows a flattened source structure. Using a two-dimensional Gaussian fit to the continuum, we obtained a total integrated flux density of 0.11 Jy, a deconvolved source size of 4.7″ × 2.9″ (P.A. = 83.1°), and a peak position of R.A.(J2000) = 05^{h}01^{m}40.^{s}086, Dec.(J2000) = +47°07′20.″90. The positional uncertainty due to noise can be estimated by $\triangle\theta = 0.45\ \frac{\theta_{\rm FWHM}}{\rm S/N}$, where $\theta_{\rm FWHM}$ is the angular resolution and S/N is the signal-to-noise ratio (Reid et al. 1988; Chen et al. 2006; Weintroub et al. 2008; Qin et al. 2010). The estimated positional uncertainty is approximately 0.″14. If we also consider the uncertainty from the Gaussian fit to the position of the continuum peak and the pointing error, then ΔR.A. = ±0.24″ and ΔDec. = ±0.21″. The 1.3 mm continuum emission is associated with an H_2O maser (Migenes et al. 1999) as well as a near-IR source detected by Varricatt et al. (2010). In addition, the peak of the 1.3 mm continuum agrees well with those of the 1.3 cm, 3.6 cm and 7 mm emission within the positional uncertainty (Sánchez-Monge et al. 2008). Sánchez-Monge et al. (2008) argued that these radio emission could be from either radio jets or hypercompart HII regions. The rising spectral index (Sánchez-Monge et al. 2008), association with an H_2O maser, and compact source structure suggest a hypercompact HII region in this region (Sewilo et al. 2004). Therefore the 1.3 mm continuum emission may comprise free-free emission from the hypercompart HII region and the thermal emission from the warm dust from its surroundings (Keto et al. 1988 & Beltrán et al. 2011). The emission from the free-free component of the continuum flux in our source can be estimated by $S_\nu \propto \nu^\alpha$, where the free-free spectral index α is 1.1 from 3.6 to 1.3 cm continuum emission. The contribution of the free-free emission to the 1.3 mm continuum is ∼ 4.4 mJy (much lower than our total integrated flux 0.11 Jy at 1.3 mm), and then can safely be ignored.

In order to determine the total gas mass of the continuum source, we make the optically thin approximation for the dust continuum emission. The total gas mass of the continuum source can be estimated by $M_{\rm core} = S_\nu D^2/\kappa_\nu R B_\nu(T_d)$, where S_ν is the flux at the frequency ν and D is the distance to the source. We assume $\kappa_\nu = 0.05(\nu/230)^\beta$ m^2 kg^{-1} for the opacity (Testi & Sargent 1998), where we adopt $\beta = 2$ (Drain & Lee 1984) and a dust-to-gas mass ratio $R = 0.01$ (Lis et al. 1991). $B_\nu(T_{\rm d})$ is the Planck function for a dust temperature T_d at frequency ν. Using a dust temperature of ∼ 30 K (Sánchez-Monge et al. 2008), we derive total gas mass = 13 $M_\odot$. Because the extended envelope can be filtered by the interferometers (missing short spacing data), the mass of the gas derived from our data is smaller than 23 $M_\odot$ from the single dish observations (Sánchez-Monge et al. 2008).

3.2. Molecular Line Emission

Figure 2 shows the spectra of ^{12}CO(2 − 1), ^{13}CO(2 − 1) and C^{18}O(2 − 1) emission at the peak position of the continuum image. The ^{12}CO(2 − 1) and ^{13}CO(2 − 1) lines present asymmetric profile with double peaks which can be caused by large optical depth (André et al. 1999 & Belloche et al. 2002). The C^{18}O(2−1) line with a single emission peak can be considered as optically thin; Hence it can be used for determination of the systemic velocity. We measure a systemic velocity of ∼ −17.0 km s^{-1} from this line. The velocities of the blue and red emission peaks of ^{12}CO(2 − 1) are −20 km s^{-1} and −13 km s^{-1}. For ^{13}CO(2 − 1), the velocities of the blue and red emission peaks are −19 km s^{-1} and −16 km s^{-1}.

The ^{12}CO(2 − 1) and ^{13}CO(2 − 1) spectra show "blue profile" signature (Wu et al. 2007), and the blue peaks of both lines are stronger than their red peaks with an absorption dip near the systemic velocity, which can be produced by infall motion or accretion. In addition, the ^{12}CO(2 − 1) spectrum show an unusual full width of ∼30 km s^{-1}, from −38 to −8 km s^{-1}. Such a broad wing is a strong indication of outflow motion.

To determine the velocity components and spatial extension of the outflow, we have made position-velocity (PV) diagram along the cuts at various position angles, and found that the redshifted and blueshifted components are the strongest at a position angle of −40° (40° west of north) as shown in Figure 3. The PV diagram in Fig. 3 clearly shows bipolar components. The blueshifted and redshifted components have obvious velocity gradients from −24.2 to −20 km s^{-1} and −13 to −8.5 km s^{-1} respectively (see the blue and red vertical dashed lines in Fig. 3). The distributions of redshifted and blueshifted velocity components in Fig.3 provide us further evidence for the bipolar outflow in this region (Yamashita et al. 1989).

Table 1. The physical parameters of the outflow.

Wing	Velocity interval km s^{-1}	Deconvolved sizes arcsec × arcsec	T_{mb} K	T_{ex} K	τ	N_{H_2} ($\times10^{21}$cm^{-2})	M_{out} ($M_\odot$)	t_d ($\times10^4$yr)	M_{out} ($\times10^{-5}M_\odot$ yr^{-1})
Blue	-24.2 to -20.0	9.9×4.3(P.A.=-60.5°)	10.0	15.2	3.7	3.1	0.4	1.9	2.1
Red	-13.0 to -8.5	13.3×5.2(P.A.=-22.5°)	7.8	12.8	3.3	6.5	1.4	1.5	9.3

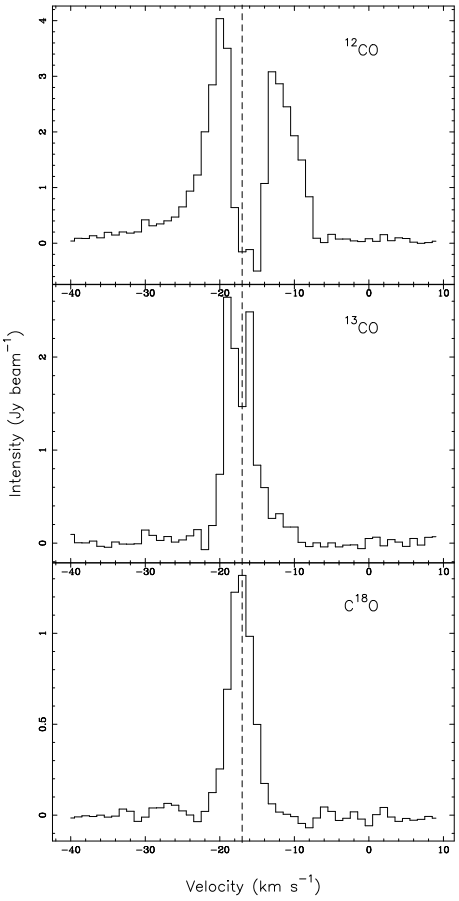

Fig. 2. Spectral profiles observed at the central position of IRAS 04579+4703 in the optically thick ^{12}CO(2−1), ^{13}CO(2−1) lines, and the optically thin C^{18}O(2 − 1) line. The dotted line in the spectra marks the cloud systemic velocity.

Using the velocity ranges determined from the PV diagram, we made the velocity integrated intensity maps superimposed on the 1.3 mm continuum as shown in Fig. 1. The blueshifted and redshifted components are presented as blue and red contours. The map clearly shows northwest-southeast bipolar components centered at the peak position of the 1.3 mm continuum. The blueshifted and redshifted lobes are not in a straight line. The outflow is associated with infrared source IRAS 04579+4703 and a near-IR source.

4. DISCUSSION

4.1. Outflow Kinematics and Driving Source

The velocity integrated intensity map, PV diagram and the broad wing (full width = 30 km s^{-1}) of the CO ^{12}CO(2 − 1) line clearly show a bipolar outflow in IRAS 04579+4703 region. The blueshifted and redshifted lobes do not lie in a straight line, and the extension is similar to that of H_2 knots (Varricatt et al. 2010), indicating that the H2 and CO most likely represent the same outflow, and that the ^{12}CO(2 − 1) outflow gas probably

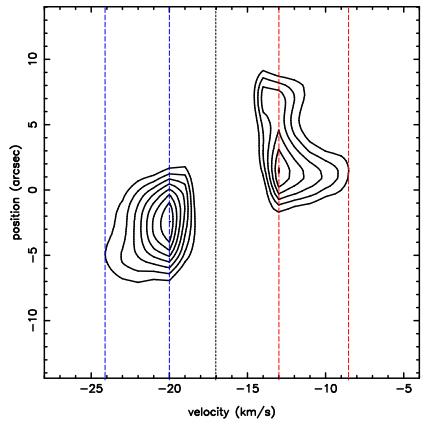

Fig. 3. The position-velocity plot of the ^{12}CO(2 − 1) emission at a position angle of −40°. The contour levels are 1.4, 1.8, 2.3, 2.7, 3.2, 3.6, 4.1 and 4.5 Jy beam^{-1}. 1 σ is 0.7 Jy beam^{-1}. The black vertical dashed line marks the cloud systemic velocity. The blue and red vertical dashed lines mark the velocity ranges of the blueshifted and redshifted emission, respectively.

is entrained by the H_2 jet-like outflow. The outflow is associated with the infrared source IRAS 04579+4703 and a near-IR source. Varricatt et al. (2010) suggested that the near-IR source may be the near-IR counterpart of IRAS 04579+4703 with the strong infrared excess. The position of the near-IR source agrees well with the peaks of the 1.3 mm, 7 mm, 1.3 cm and 3.6 cm emission within the positional uncertainty. H2 and Brγ emission are very close to the near-IR source (Ishii et al. 2001 & Varricatt et al. 2010). Together, we conclude that the near-IR source may be an embedded massive YSO, which is likely to drive the bipolar outflow.

Under conditions of local thermodynamical equilibrium (LTE), ^{12}CO(2-1) being optically thick, and the completely filling beam with the source (the filling factor $f = 1$), the column density of the outflow is estimated by using the equation (eq. 1) following Garden et al. (1991) with a relation $N_{H_2} \approx 10^4 N_{^{12}CO}$(Dickman 1978):

$$N_{H_2} = 1.08\times10^{17} \frac{(T_{ex}+0.92)}{\exp(-16.62/T_{ex})} \int T_{mb} \times \frac{\tau dv}{[1-\exp(-\tau)]} \mathrm{cm}^{-2}, \quad (1)$$

where T_{ex} is the excitation temperature, T_{mb} is the corrected main beam temperature, and τ is the optical depth for the ^{12}CO(2-1) line. We assume the solar abundance ratio [^{12}CO]/[C^{18}O]=τ(^{12}CO)/τ(C^{18}O)=490 (Garden et al. 1991). T_{ex} is estimated following the equation $T_{ex} = 11.1/\ln[1 + 1/(T_{mb}/11.1 + 0.02)]$ (Garden et al. 1991). The red and blue lobes of the outflow peak near the continuum, then we assume that the ^{12}CO and C^{18}O trace same cloud components in the peak positions of the two lobes for the calculation, the assumption is reasonable since both ^{12}CO(2 − 1) and C^{18}O(2 − 1) are low energy transition with similar upper level energy. Under assumption of C^{18}O being optically thin, we calculate τ according to $\tau = -490\ln[1 - (e^{11.1/T_{ex}} - 1)T^{18}_{mb}/11.1]$ (Garden et al. 1991). Under the Rayleigh-Jeans approximation, 1 Jy beam^{-1}

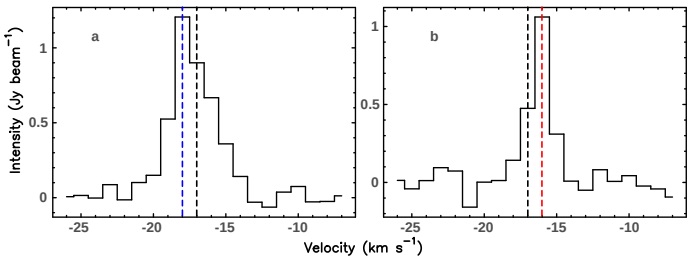

Fig. 4. $C^{18}O(2-1)$ spectra. In a and b panels, the molecular spectra are extracted from the positions of the blue and red plus symbols marked in Fig. 1, respectively, which are separated by 4″. The black vertical dashed line marks the cloud systemic velocity. The blue and red vertical dashed lines mark the peak velocities, respectively.

in our SMA observations corresponds to a brightness temperature of 2.52 K. Furthermore, the mass of the outflow is given by $M_{\rm out} = mN_{\rm H_2}S/(2.0\times10^{33})$ $M_\odot$, where m is 1.36 times the H_2 mass (Garden et al. 1991) and S is the size of each lobe. S is obtained from the deconvolved lobe size (In Table 1). A dynamic time scale can be determined by $t_d = r/v$, where v is the maximum flow velocity relative to the cloud systemic velocity , and r is the length of the begin-to-end flow extension for each lobe. The lengths of the blueshifted and redshifted lobe are 0.14 pc and 0.13 pc obtained from Fig.1, respectively, which is only a lower limit due to projection on the sky plane. The mass entrainment rate of the outflow is calculated using $\dot{M}_{\rm out} = M_{\rm out}/(t_{\rm d})$. The physical parameters and the calculated results of the outflow are summarized in Table 1. The parameter difference of the two lobes reflects that the ambient material is not uniform and then the entrained masses and dynamics are different. The outflow has the total mass of 1.8 $M_\odot$ and the mass entrainment rate of 1.1×10^{-4} $M_\odot\,yr^{-1}$. The average dynamical timescale is about 1.7×10^4 yr.

4.2. Accretion

Our interferometric continuum image toward IRAS 04579+4703 reveals a flattened structure, perpendicular to the direction of the outflow detected in $^{12}CO(2-1)$ and H_2, which is consistent with accretion disk scenario observed in the other high mass star formation regions (Cesaroni et al. 1999; Shepherd et al. 2001; Patel et al. 2005). The $C^{18}O(2-1)$ spectra from the two positions (the red and blue plus symbols in Fig. 1) perpendicular to the direction of the outflow are shown in Figure 4. The velocity gradient is seen from the $C^{18}O(2-1)$ spectra, suggesting that the disk is rotationally and gravitationally bound by the central YSO. Assuming the rotation is Keplerican, the dynamical mass (binding mass) is estimated by $M = \delta v^2 r/G\sin^2(i)$, where r is the half spatial separation of the emission, δv is the difference between the peak velocity of the emission and the systemic velocity, and i is the unknown inclination angle between the disk plane and the plane of the sky ($i = 90^\circ$ for an edge-on system). Adopting the values $r \sim 2''$ and $\delta v \sim 1$ km s^{-1} shown in Figures 1 and 4, the obtained dynamical mass is $\sim 6/[\sin^2(i)]M_\odot$. The dynamical mass is estimated to be 12 $M_\odot$ if $i = 45^\circ$, which is a lower limit since that we estimated the binding mass from the kinematics inside 2″ due to our low spatial resolution observations.

The spectroscopic observations of H_2 and Brγ (Ishii et al. 2001) also suggested the presence of an accretion disk, and this source is probably accreting. If we assume that the central star is a massive protostar and not in the phase of zero-age main-sequence (ZAMS) star, then the bolometric luminosity ($3.91\times10^3 L_\odot$) is equal to accretion luminosity. According to Molinari et al. (1998b), the accretion rate is given by $\dot{M} = 6.22\times10^{-9}(L/L_\odot)^{1.70}(M/M_\odot)^{-1.24}$. Assuming the dynamical mass of 12 $M_\odot$ is equal to the protostar mass, the expected accretion rate is 3.7×10^{-4} $M_\odot$yr^{-1}.

The "blue profile" of the $^{12}CO(2-1)$ line provide a further evidence for infall motion or accretion as discussed in section 3.2. The mass accretion rate is estimated by $\dot{M} = 4\pi R^2 Vmn$ (Myers et al. 1996), where m is 1.36 times the H_2 mass. If cloud core is approximately spherical in shape, the mean number density is $n = 1.62\times10^{-19}N_{\rm H_2}/L$, where L is the cloud core diameter in parsecs, which is 0.056 pc (the major axis of the deconvolved size of the continuum). $N(H_2)$ is the column density of molecular hydrogen obtained from the equation (eq. 3) of Xu et al. (2010) in $C^{18}O$ line. The velocity difference (V) of 2.0 km s^{-1} between the systemic velocity (-17.0 km s^{-1}) and the velocity of the redshifted absorbing dip (-15.0 km s^{-1}) and a source size (R) of 0.028 pc, then we obtain a mass accretion rate of $\sim 2.3\times10^{-4}$ $M_\odot$yr^{-1} which is roughly consistent with the value derived from bolometric luminosity, further suggesting the presence of an accretion disk in this region, but the observations at the current spatial resolution are not adequate to distinguish the disk accretion and the observations of more molecular tracer with higher spatial resolutions are needed to resolve detailed kinematics in this region.

Acknowledgements. We thank the anonymous referee for his/her constructive comments and suggestions that greatly improved the content and presentation of this paper. Jin-Long Xu's research is in part supported by 2011 Ministry of Education doctoral academic prize.

References

André, P., Motte, F., & Bacmann, A. 1999, ApJ, 513, L57
Belloche, A., André, P., Despois, D., & Blinder, S. 2002, A&A, 393, 927
Beltrán, M. T., Cesaroni, R., Neri, R., & Codella, C. 2011, A&A, 525, 151
Beuther, H., Hunter, T. R., & Zhang, Q. 2004, ApJ, 616, 23
Cesaroni, R. et al. 1999, A&A, 345, 949
Chen, H.-R., Welch, W. J., Wilner, D. J., & Sutton, E. C. 2006, ApJ, 639, 975
Dickman, R. L. 1978, ApJ, 37, 407
Draine, B. T., & Lee, H. M. 1984, ApJ, 285, 89
Furuya, R. S., Cesaroni, R., & Shinnaga, H. 2011, A&A, 525, 72
Garden P. R., Hayashi M., Hasegawa T., et al. 1991, ApJ, 374, 540
Ishii, M., Nagata, T., Sato, S., et al. 2001, AJ, 121, 3191
Jiang, Z., et al. 2005, Nature, 437, 112
Keto, E. R., Ho, P. T. P., & Haschick, A. D. 1988, ApJ. 324, 920
Lang, K. R. 1980 Aatrophysical formulae (Berlin: Springer-Verlag).
Lis, D. C., Carlstrom, J. E., & Keene, J. 1991 ApJ, 380, 429
Migenes, V., Horiuchi, S., Slysh, V. I., et al. 1999, ApJSS, 123, 487
Molinari, S., Brand, J., Cesaroni, R., & Palla, F. 1996, A&A, 308, 573
Molinari, S., Brand, J., Cesaroni, R., Palla, F., & Palumbo, G. G. C., 1998a, A&A, 336, 339
Molinari, S., Testi, L., Brand, J. et al., 1998b, ApJ, 505, L39
Myers, P. C., Mardones, D., Tafalla, M., et al. 1996, ApJ, 465, L133
Palla, F., Brand, J., Comoretto, G., Felli, M., & Cesaroni, R. 1991, A&A, 246, 249
Patel, N. A., et al. 2005, Nature, 437, 109
Qin, S.-L., Zhao, J.-H., Moran, J. M. 2008, ApJ, 677, 353
Qin, S.-L., Wu, Y. F., Huang, M. H., et al. 2010, ApJ, 711, 399
Reid, M. J., Schneps, M. H., Moran, J. M., et al. 1988, ApJ, 330, 809
Sánchez-Monge, Á., Aina, P., Estalella, R., Beltrán, M. T., & Girart, J. M. 2008, A&A, 485, 497
Sewilo, M., Churchwell, E., Kurtz, S., et al., 2004, ApJ, 605, 285
Shepherd, D., Claussen, M. J. & Kurtz, S. E. 2001, Science, 292, 1513
Shu, F. H., Adams, F.C., & Lizano S. 1987, ARA&A, 25, 23
Testi, L., & Sargent, A. I. 1998, ApJ, 508, L91
Varricatt, W. P., Davis, C. J., Ramsay, S., & Todd, S. P. 2010, MNRAS, 404, 661
Weintroub, J., Moran, J. M., Wilner, D. J., et al. 2008, ApJ, 677, 1140
Wouterloot, J. G. A., & Brand, J. 1989, A&AS, 80, 149
Wu, Y., Henkel, C., Xue, R., Guan, X., & Miller, M. 2007, ApJ, 669, L37

Xu, J.-L., & Wang, J.-J. 2010, RAA, 10, 151
Yamashita, T., Suzuki, H., Kaifu, N., et al. 1989, ApJ, 347, 894
Zhang, Q., Hunter, T. R., Brand, J., et al. 2005, ApJ, 625, 864
Zinnecker, H., Yorke, H. W. 2007, ARA&A, 45, 481